Groundwater

Methods Note/

Improved Method for Simulating Groundwater Inundation Using the MODFLOW 6 Lake **Transport Package**

by Lauren K. Mancewicz¹, Alex Mayer², Christian Langevin³, and Jason Gulley⁴

Abstract

Groundwater inundation due to sea level rise can affect island and coastal freshwater resources by exposing water tables to direct, continuous evaporation. Numerical simulations of groundwater inundation effects on coastal and island aquifers have been limited by an inability to simulate solute transport and variable density flow between the aquifer and lakes formed by groundwater inundation. Consequently, we contributed to the development of a new tool, the Lake Transport Package, for MODFLOW 6 that can calculate solute concentrations within lakes and allows for variable density flow between lakes and aquifers. Here we use groundwater inundation as an example application to showcase the functionality of the Lake Transport Package and the advantages of using this tool over past methods of representing groundwater inundation. We developed hypothetical island simulations based on hydrogeological characteristics of the Bahamas. Multiple sea level rise and lake evaporation rates were simulated to evaluate the effects of groundwater inundation on freshwater lens size for different climates. The results demonstrate the ability of the Lake Transport Package to calculate the solute concentration of the lake for transient simulations, including hypersaline concentrations. Higher sea level rise and greater lake evaporation rates lead to a greater loss of the freshwater lens and higher lake salinity. The formation of a lake and corresponding expansion due to groundwater inundation increases the loss of freshwater by 6-36%, depending on the lake evaporation rate. These simulations validate the performance and demonstrate usefulness of the Lake Transport Package as a tool in representing groundwater inundation.

Introduction

Groundwater inundation due to sea level rise and the effects on freshwater resources has been the focus

Received March 2022, accepted September 2022. © 2022 National Ground Water Association. doi: 10.1111/gwat.13254

of recent work (Bjerklie et al. 2012; Rotzoll and Fletcher 2013; Masterson et al. 2014; Gulley et al. 2016; Habel et al. 2017), yet a more complete understanding of groundwater inundation has been limited. Groundwater inundation occurs when the groundwater table rises above land surface causing flooding. The emerging significance of groundwater inundation and its effects on freshwater provides motivation for the development of new modeling tools to address this phenomenon and its effects on the freshwater lens. MODFLOW 6, the most recent version of MODFLOW, is a widely used numerical groundwater modeling program maintained by the U.S. Geological Survey (Hughes et al. 2017; Langevin et al. 2021). This work aims to demonstrate the functionality and advantages of using the variable density capabilities in MODFLOW 6 (Langevin et al. 2020) with the recently created Groundwater Transport Model (Langevin et al. 2022).

NGWA.org

¹Corresponding author: Department of Civil, Environmental and Geospatial Engineering, Michigan Technological University, 1400 Townsend Dr., Houghton, MI 49931; Ikmancew@mtu.edu

²Department of Civil Engineering, University of Texas at El Paso, El Paso, TX

³Earth Systems Modeling Branch, U.S. Geological Survey, Mounds View, MN

⁴School of Geosciences, University of South Florida, Tampa, FL Article impact statement: The development of a tool for modeling lake-groundwater interactions is applied to address the emerging problem of groundwater inundation.

The Groundwater Transport Model includes the Lake Transport Package, which calculates changes in solute concentration within individual lakes based on solute budget calculations. These new capabilities are applied to simulate groundwater inundation for an island setting.

In a homogeneous island aquifer, fresh groundwater occurs in a characteristic convex shape due to the density differences between fresh and salt water (see Figure 1A). This accumulation of fresh groundwater is known as the freshwater lens. The Ghyben-Herzberg equation (Ghyben 1889; Herzberg 1901) relates the depth of the freshwater lens below sea level (z) to the elevation of the water table above sea level (h) at equilibrium:

$$z = \alpha h \tag{1}$$

where α is a density ratio defined as:

$$\alpha = \frac{\rho_f}{\rho_s - \rho_f} \tag{2}$$

where ρ_f is the density of fresh groundwater and ρ_s is the density of saline groundwater. For typical densities of fresh and saline water of 1000 and 1025 kg/m³, respectively, the depth of the freshwater lens below sea level is 40 times the height of the water table above sea level. Additionally, the hydrogeologic characteristics of the island-aquifer system, such as the hydraulic conductivity distribution, island size and topography, and net recharge rates influence the water table and extent of the freshwater lens.

Sea level rise and reductions in aquifer recharge, from climate change can negatively affect the freshwater lens, reducing the amount of fresh groundwater available for water supplies. As sea level rises, coastal areas can become inundated, decreasing island widths and shortening lateral groundwater flowpath lengths, which in turn decrease the water table elevation relative to sea level (Gulley et al. 2016). According to the Ghyben-Herzberg ratio, the corresponding decrease in the depth to the base of the freshwater lens is 40 times the change in water table height. Thus, even a small change in the water table elevation can have a significant effect in the thickness of the freshwater lens. In addition to raising sea level, climate change may alter precipitation patterns and evapotranspiration rates, resulting in a loss of net recharge and further decreasing the freshwater lens size.

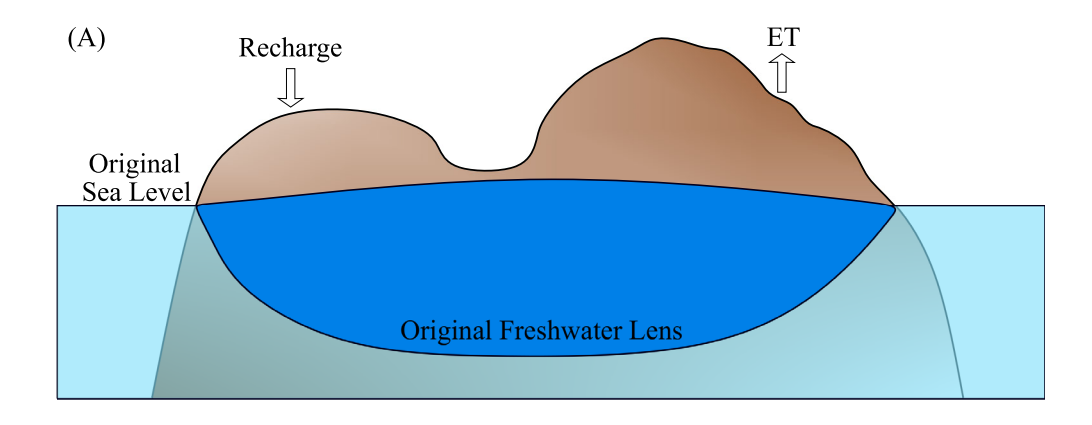
Groundwater inundation is an additional mechanism for freshwater lens depletion (see Figure 1). As sea level rises, the freshwater lens moves upwards, potentially flooding low-lying areas and expanding existing lakes and wetlands, or even creating new surface water features. For the groundwater lying below land surfaces, the effective recharge rate (precipitation rate minus evapotranspiration rate) is typically positive. However, if the groundwater is hydraulically connected to surface water, it is exposed to a negative effective recharge if the lake evaporation rate exceeds the precipitation rate. In this case, the surface water body essentially acts as a pump depleting the fresh groundwater lens (Gulley et al. 2016).

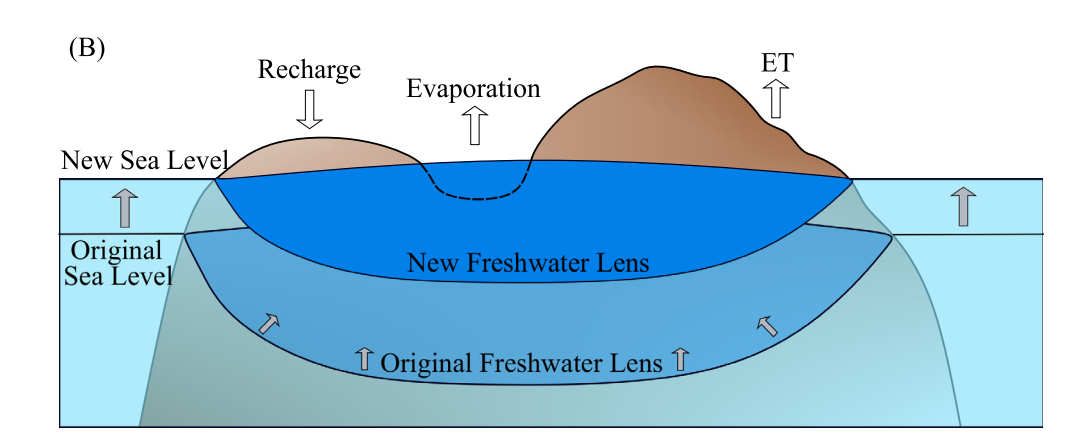
In recent work, Gullev et al. (2016) simulated groundwater inundation in a hypothetical island under steady state conditions with SEAWAT, a commonly used variable-density coupled groundwater flow and transport program (Guo and Langevin 2002; Langevin et al. 2008). Because SEAWAT lacks the ability to model lakes directly, Gulley et al. (2016) represented a lake as a series of cells at the top of the aguifer with high hydraulic conductivity (K) relative to the surrounding aguifer and 100% porosity. The intention of this approach was to allow flow and solute exchange between the lake cells and the aquifer cells, while generating constant heads in the lake cells such flow was insignificant within the lake cells. To model the effect of sea level rise and the associated groundwater inundation and lake expansion using this "high-K" approach, the user must determine the lateral extent of the lake cells for each combination of sea level rise rate, lake bathymetry, and elapsed time. The lateral extent of the lake cells is computed external to the SEAWAT model and the input files for the aguifer properties and boundary conditions must be adjusted accordingly.

While application of the "high-K" approach has provided insights to the relative effect of sea level rise and groundwater inundation on island freshwater lenses, this approach has some limitations. First, the approach method requires the user to perform external calculations and manually update boundary conditions and aquifer property input files, as well as complete additional post processing to obtain flow and transport budgets for the lake (Hunt et al. 2003). Additionally, numerical conditions in the lake cells can potentially lead to longer run times and result in unrealistic spatial gradients in hydraulic head and salinity (Merritt and Konikow 2000; Mulligan et al. 2011). These gradients can affect the flux of water and solute into and out of the lake thereby affecting the lake salinity and the surrounding groundwater. Furthermore, the high-K approach can lead to numerical instability due to the several orders of magnitude difference in hydraulic conductivity between lake and aquifer cells that are adjacent to one another (Merritt and Konikow 2000; Mulligan et al. 2011).

The original MODFLOW Lake Package calculates lake stage and volume from the lake water balance, which includes Darcy-flux-based exchange between the lake and the aquifer (Cheng and Anderson 1993). Later versions included improved solution methods and incorporated additional lake characteristics such as irregular bathymetry that allows for lakes to coalesce depending on the stage and for a lake to dry and rewet (Council 1997; Merritt and Konikow 2000; Langevin et al. 2017). Additionally, the Lake3 Package has the ability to simulate solute exchange between a lake and the aquifer when used with MOC3D, a solute transport model compatible with previous versions of MODFLOW (Konikow et al. 1996; Merritt and Konikow 2000).

The ability to simulate solute transport between a lake and the aquifer, as done with the Lake3 Package, is critical for being able to represent groundwater inundation.





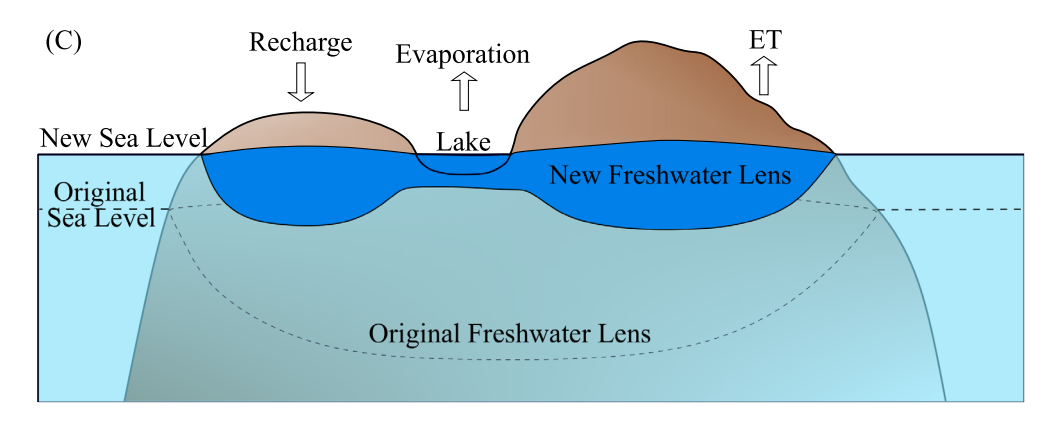


Figure 1. Process of groundwater inundation due to sea level rise for an island, where ET is evapotranspiration. (A) Shows the original freshwater lens and sea level prior to sea level rise. As the sea level rises, the freshwater lens also rises, flooding low lying areas (B). The newly formed lake exposes what was once fresh groundwater to evaporation, increasing freshwater lens losses and decreasing the freshwater lens volume (C).

In this paper, we extend previous work on MODFLOW lake packages by implementing lake transport processes into the MODFLOW 6 framework. This allows us to take advantage of recent MODFLOW advances, not available in previous MODFLOW versions, that are beneficial for representing groundwater inundation. For example, the MODFLOW 6 Lake Package supports the Newton formulation, which improves numerical convergence for layer wetting and drying conditions commonly encountered in island settings due to sea level fluctuations. Additionally,

while not used in our study, MODFLOW 6 supports unstructured grids whose flexibility is beneficial for efficiently discretizing irregularly shaped islands. Also, MODFLOW 6 supports multispecies simulations where different species (e.g., nutrients, tracers, heat) can be incorporated in an equation of state for density, affecting flow between the lake and aquifer. Also, when using the Buoyancy Package in MODFLOW 6 along with the Lake Transport Package, both solute transport between the lake and aquifer and variable density flow can be accounted

for (Langevin et al. 2022). By combining the Lake Package and the Lake Transport Package, MODFLOW 6 provides a way to model groundwater inundation in a way that is more physically accurate while overcoming the limitations encountered with using SEAWAT and the high-K approach.

The Lake Package is a head-dependent flux boundary package within the Groundwater Flow Model that calculates water fluxes between a lake and the aquifer (Langevin et al. 2017). The stage of the lake is calculated according to changes in the flow budget for the lake. As the lake stage changes, the lake surface area is recalculated according to bathymetry specified by the user. Consequently, lake flux boundary conditions, such as precipitation and evaporation, are automatically adjusted to reflect the change in lake surface area. As the lake expands, cells with aquifer boundary conditions are reassigned to lake conditions. As the lake contracts, former lake cells are converted to aquifer cells with aquifer boundary conditions (Langevin et al. 2017). These flow and stage changes are recalculated for each Picard iteration loop; the solution is not considered converged until these changes are less than user-specified tolerances. Using the Lake Package in MODFLOW 6 to represent a lake, as opposed to the high-K approach with SEAWAT, eliminates the need for external calculations of lake stage and extent of the lake. Additionally, the Lake Package does not require boundary conditions and aquifer properties to be manually updated with external calculations as they do with the high-K approach. These features of the Lake Package allow for sea level rise-lake expansion simulations to be run straightforwardly with a single simulation.

Methods

Representing Groundwater Inundation Using the Lake and Lake Transport Packages

The recently developed MODFLOW 6 Lake Transport Package is part of the Groundwater Transport Model and has been successfully tested with existing constant density lake transport examples (Langevin et al. 2021). The Lake Transport Package accommodates transport and variable density flow into and out of the lake. The concentration of the solute in the lake is calculated with the following mass balance, assuming instantaneous and uniform mixing within the lake:

$$C^{i} = \frac{C^{i-1}V^{i-1} + \sum_{j} Q^{i}_{j}C^{i}_{j}\Delta t}{V^{i}}$$
 (3)

where C is the solute concentration in the lake at the current (i) or previous (i-1) time step, j is the lake cell index at time i, V is the volume of the lake, Q_j is the flux into or out of the lake cells associated with the aquifer, and C_j is the solute concentration in the lake cells associated with the aquifer for flux out of the lake or the solute concentration in the aquifer cells associated with the lake for flux into the lake, and Δt is the duration of the time

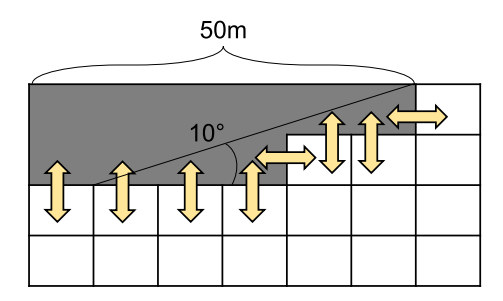


Figure 2. General geometry of the lake showing the designation of the lake connection cells. The size of the cells is not to scale, but instead show the relative setup of the lake for the Lake Package. The lake is indicated in gray and consists of inactive cells. Connections between the lake and aquifer can be vertical, horizontal, or both as indicated by the arrows.

step. Additionally, the Lake Package for flow and the Lake Transport Package are capable of accommodating the effects of density variations by implementing a variable density form of Darcy's Law based on hydraulic head (Langevin et al. 2020). The code for the Lake Transport Package is available as part of the Groundwater Transport Model for MODFLOW 6 (Langevin et al. 2021).

Example Island with a Lake and Sea Level Rise

To demonstrate the functionality of the Lake and Lake Transport Packages, within the context of sea level rise and groundwater inundation on an island, we created a two dimensional (2D) variable density flow and transport model for a hypothetical 1000 m wide strip island. MODFLOW 6 version 6.2.2 (Langevin et al. 2021) was used with FloPy (Bakker et al. 2021), a Python package used to create the MODFLOW input files, run simulations, and post process results. The hydrogeologic properties and conceptual model for these simulations were based on the carbonate platform islands of the Bahamas, similar to Gulley et al. (2016) (Table 1). Due to the symmetry of the hypothetical island, only half of the island was modeled, resulting in a 500 m wide domain. The top of the domain was set to 4.4 m above sea level (ASL) and the bottom to -40.6 m ASL with cell dimensions of 2 m in the lateral direction by 1 m in the vertical direction. We defined freshwater as having a solute concentration equal to or less than 1.0 g/L and the freshwater lens size was defined as the total number of freshwater cells at a given timestep divided by the initial number of freshwater cells for that simulation.

The surface topography had an area of lower elevation located at the center of the island. As sea level rose in transient simulations, this depression became inundated with groundwater, forming a half lake. The depression was 50 m wide along the bottom, which was set at an elevation of 0.4 m ASL. The lake bathymetry had a constant slope of 10° from the bottom edge of the depression to the top of the model domain (Figure 2). Vertical and horizontal lake connection cells were specified as shown in Figure 2. Aquifer cells adjacent to the lake were assigned relatively high values for the storage properties $(1.0 \text{ m}^{-1} \text{ for specific storage})$ applied

when the hydraulic head is above the cell top. These large storage values improved convergence of the flow solution as cells transitioned from partially saturated to fully saturated. We specified evapotranspiration (ET) and land surface precipitation for the uppermost active cells in the aguifer with a maximum ET rate equal to recharge (0.00055 m/d). A no-flow boundary condition was used along the bottom and left edge of the domain. The coastal boundary was represented with a vertical face along the right side of the model domain using the general head boundary (GHB) package with salinity equal to sea water (35 g/L). The hydraulic head was set equal to sea level and the conductance was set to 20 m²/d. To generate initial conditions, we ran a spin up simulation with sea level (GHB head) set to 0 m and all other boundary conditions as specified above. We ran the spin up simulation until the consecutive change in the average salinity was less than 10^{-6} g/L and the maximum change in salinity for a single cell was less than 10^{-10} g/L. A timestep of 5 d with one stress period was used for the spin up simulation and the solution resulted in the lake being dry with the water table below the bottom of the lake. Additional hydrologic parameters are shown in Table 1.

We ran eight transient simulations with varying sea level rise rates and effective recharge rates for a total duration of 200 years with a time step of 5 d, using the spin up results as the initial condition for each simulation (Table 2). We used a high and a low sea level rise rate of 0.01 m/year (1 m/100 year) and 0.02 m/year (2 m/100 year), respectively. Sea level rise

Table 1
Values Used for Aquifer Properties and Model
Domain Setup

Value
$2 \times 1 \times 1$
4.4
-40.6
500
20
20
0.008, 1.0 for lake connection cells
0.30
1.0
0.1
0.00055
0.00055
2.0
0.00055
Varied; 0.0019, 0.0011, 0.0006
1.0
4.0

¹ SURFDEP is a smoothing parameter used to represent depressions in the bottom surface of a lake that can also aid in convergence.

was represented by changing the hydraulic head in the GHB condition within MODFLOW 6. We conducted sea level rise simulations with and without a lake. For the sea level simulations with a lake, the lake rainfall and evaporation rates were 5.5×10^{-4} m/d and 6.6×10^{-4} m/d, respectively, which are typical for the central Bahamian islands (Gulley et al. 2016) and give a slight net negative water loss for the lake. We conducted two more sets of sea level rise simulations with a lake with higher evaporation rates of 1.1×10^{-3} m/d and 1.75×10^{-3} m/d to simulate hypersaline lake solute concentrations and the greater effects from upcoming of the freshwater lens underneath the lake. The flow and solute mass balance errors for all simulations were less than 0.1 and 0.01%, respectively.

Results

For the simulations with a lake, as the freshwater lens rose in parallel with sea level rise, groundwater inundated the area of low topography, increasing the lake stage (Figure 3). The lake stage increased more quickly and groundwater inundation is greater with the lower evaporation rates and high sea level rise scenario. Lower evaporation rates resulted in smaller losses from the lake water budget compared to higher evaporation rates and a greater lake stage. With higher evaporation rates, more water was lost from the lake, which reduced the lake stage. As sea level rose, so did the freshwater lens and the water table. Thus, higher sea level rise rates also increased the lake stage more quickly because the freshwater lens and water table were also rising at a quicker rate. Additionally, the rate of change in lake stage relates to the rate of change in lake salinity (Figure 4). As the lake stage increased, the lake expanded increasing the lake surface area. As the surface area increased, the amount of water lost from evaporation also increased, raising the lake salinity. Directly increasing the evaporation rate similarly increases the lake salinity.

In the case of extreme lake evaporation $(3.5 \times \text{recharge})$ and a rate of $0.02\,\text{m/year}$ for sea level rise, unstable miscible displacement appears to occur (Figure 5). Unstable miscible displacement similarly occurred in the extreme lake evaporation with a low sea level rise rate simulation at year 128 and the high lake evaporation with a low and high sea level rise rate simulation at year 172 and 120, respectively. For the extreme evaporation rate scenario, several other timesteps had unstable miscible displacement that occurred to a much lesser extent and did not appear to substantially affect the lake salinity.

The loss of surface freshwater from lake evaporation not only affected the lake salinity, but also the extent of the fresh groundwater lens. Depending on the lake evaporation rate, the presence of a lake increased the loss of freshwater from the freshwater lens over the 200-year simulation period by 6.1 to 36.2% and 6.54 to 14.5% relative to an island without a lake, with sea level rise rates of 0.01 and 0.02 m/year, respectively. The higher

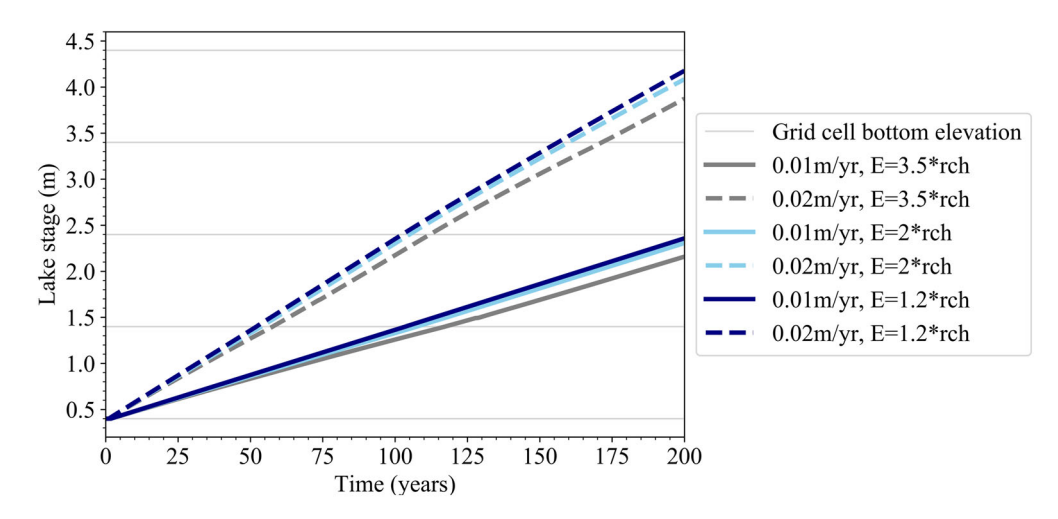


Figure 3. Change in lake stage over time for each simulation with a lake where E is the evaporation rate and rch is the recharge rate. At the beginning of each simulation, the water table starts off below the lake bottom and the lake is dry, briefly resulting in a constant lake stage at 0.4 m until the water table inundates the area of lower topography forming the lake. The elevation of the bottom of each grid cell connected to the lake is shown in gray. Once the lake stage is greater than the bottom elevation, a new row of connection cells are "turned on." The stage increases more rapidly for the high sea level rise simulations and for those with lower lake evaporation rates.

lake evaporation rates resulted in greater freshwater lens depletion (Figure 6, Table 2). The freshwater lens curves in Figure 6 are not particularly smooth due to the discrete nature of counting individual model cells that meet the freshwater criteria.

Distinct changes also were evident in the rate of freshwater lens depletion for the simulations with the higher sea level rise rate compared to the lower sea level rise rate. In the higher sea level rise rate simulations, the water table rose closer to the surface increasing ET, the rate of which varies linearly from 0 m/d at the cutoff depth of 2 m to 0.00055 m/d at the surface. As the rate of ET increased, freshwater was more quickly lost from the freshwater lens resulting in the steeper slopes of the curve observed in Figure 6 for the simulations with a sea level rise rate of 0.02 m/year. Additionally, this change in the slope shown in Figure 6 around 105 years occurs ~5 years earlier for the simulation without a lake and later for the simulation with a lake. The difference in timing resulted from freshwater being lost to the lake due to evaporation,

which slows the rise in the water table. Therefore, it takes slightly longer for the water table to reach the cutoff depth for ET. Variations in the slope of the lens depletion curves also show the effects of unstable miscible displacement. In simulations that exhibit unstable miscible displacement the depletion of the lens briefly accelerated as the finger of more saline water moves from the lake into the aquifer, as can be seen from years 165 to 175 for high evaporation with the low sea level rise simulation.

The depletion of the freshwater lens is illustrated in Figure 7, which shows the difference in the salinity cross section between the initial conditions and the final timestep for the sea level rise simulation for an island with a lake under the high sea level rise, high lake evaporation scenario. In this scenario, the final freshwater lens was only 5.78% of initial lens volume. Additionally, the freshwater lens no longer extended underneath the lake and in the case of a full island, as opposed to the half island modeled in the domain, the freshwater lens would be fractionated.

Table 2
Summary Description of the Simulations and the Results for Each at the Final Timestep

Description (lake evaporation/sea level rise rate)	Sea Level Rise Rate (m/year)	Lake Evaporation Rate Relative to Recharge	Lake Evaporation (m/d)	Final Freshwater Lens Volume (% of initial lens volume)	Final Lake Concentration (g/L)
Extreme/low	0.01	3.5× recharge	0.0019	46.9	16.8
Extreme/high	0.02	$3.5 \times \text{recharge}$	0.0019	1.79	41.6
High/low	0.01	2× recharge	0.0011	64.6	1.60
High/high	0.02	2× recharge	0.0011	5.78	14.3
Low/low	0.01	1.2× recharge	0.0006	77.0	0.02
Low/high	0.02	1.2× recharge	0.0006	9.76	1.01
No lake/low	0.01	_	_	83.1	_
No lake/high	0.02	_		16.3	_

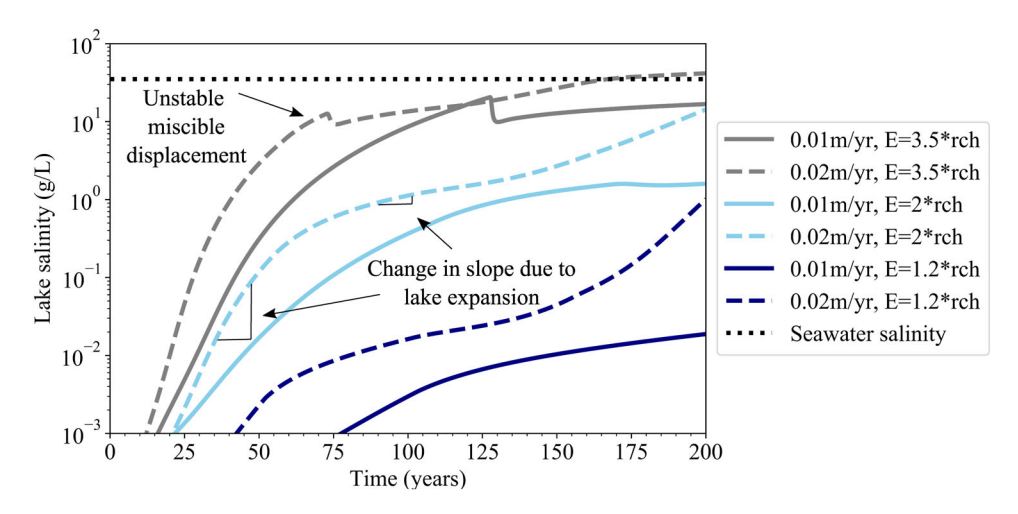


Figure 4. Change in the lake concentration as calculated by the Lake Transport Package where E is the evaporation rate and rch is the recharge rate. The concentration of sea water is also shown for reference (35 g/L). Greater evaporation and sea level rise rates result in higher concentrations. The results were truncated at 10^{-3} g/L. The annotations highlight an event of miscible displacement that affected the lake salinity and the response of lake salinity to the initial lake expansion.

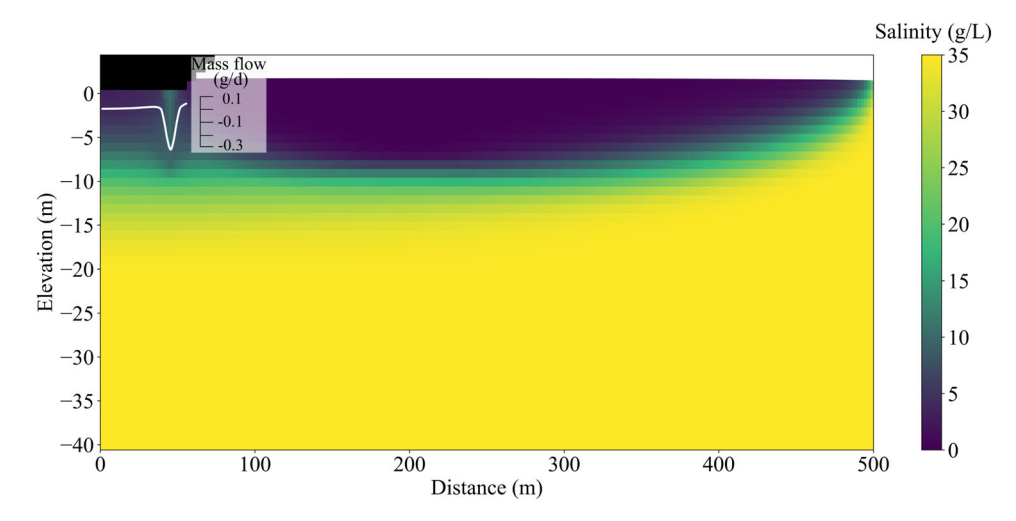


Figure 5. Concentration cross section showing unstable miscible displacement underneath the lake at 0 m elevation and 45 m from the left boundary for the extreme evaporation with high sea level rise scenario at time equal to 73 years. Elevation is shown on the y-axis and distance is shown along the bottom. The color bar shows the lake concentration in g/L with dark blue representing freshwater and yellow representing salt water. The area in black is cells that have been inactivated representing the possible extent of the lake. The white line shows the mass flow rate (g/d) from the lake to the aquifer connection cells where positive values indicate the movement of mass into the lake, and negative values represent mass moving out of the lake into the aquifer.

Discussion

In regard to unstable miscible displacement, as freshwater from the lake was lost due to excessive evaporation, salt accumulated within the lake causing instability between the two fluids resulting from the density differences between the lake and the aquifer. This results in "fingering" of denser lake water plumes protruding into the less dense groundwater. Predicting the onset of and modeling unstable miscible displacement is a difficult task, but minimizing general numerical errors and increasing dispersion (if appropriate) may be helpful when fingering occurs (Schincariol et al. 1994; Diersch and Kolditz 2002; Greskowiak 2014). In this simulation, the lake salinity dropped at approximately 70 years before

continuing to increase (Figure 4). At this point, unstable miscible displacement occurred along the right side of the lake as a finger of higher density lake water with a salinity of approximately 10 g/L moved downward underneath the lake before being diluted by the aquifer (Figure 5). Unstable miscible displacement is known to occur even for small differences in density and at low concentrations less than 10 g/L (Schincariol et al. 1994; Habtemichael et al. 2014). At the same time, the flow on the right side of the lake changed direction from into the lake to into the aquifer. Mass was lost from the lake into the aquifer connection cells at that location due to unstable miscible displacement that occurred below the lake, as shown in Figure 5, reducing the lake salinity and supporting this

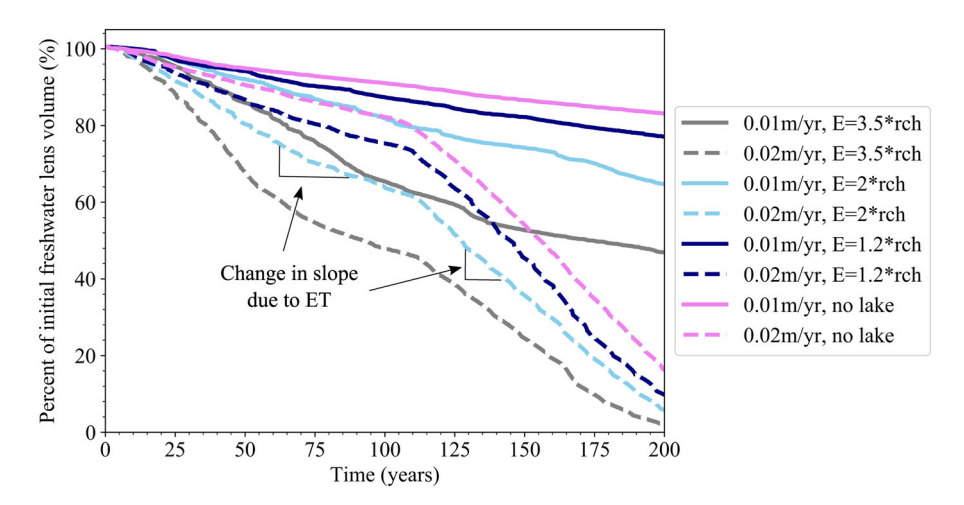


Figure 6. Freshwater lens volume as a percentage of the initial freshwater lens volume where E is the evaporation rate and rch is the recharge rate. The annotations highlight an event of miscible displacement and the response of the freshwater lens depletion rate in response to evapotranspiration (ET).

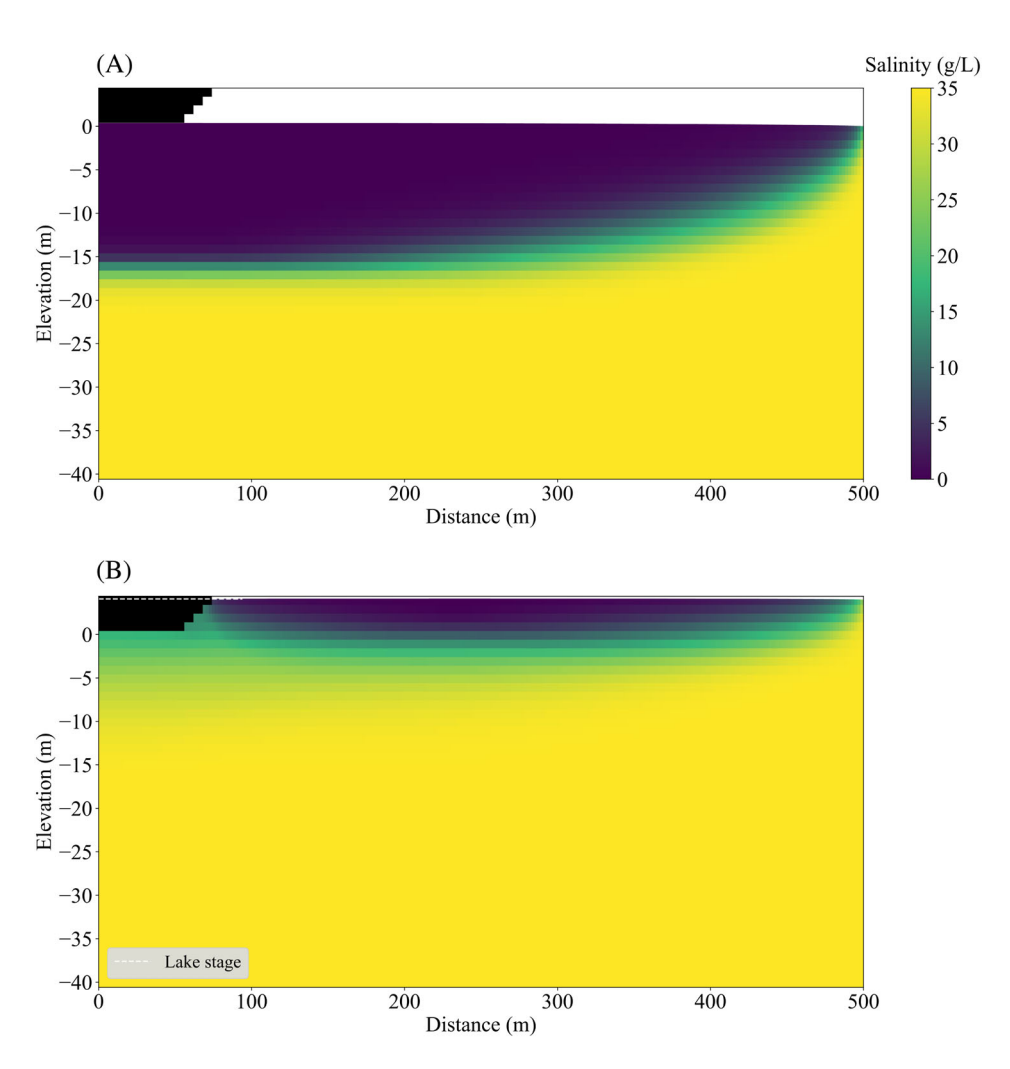


Figure 7. Concentration cross section for the high lake evaporation $(2 \times \text{ recharge})$ with a high sea level rise rate (0.02 m/year). The initial conditions are presented in A where the water table is just below the bottom of the lake and the lake is dry. (B) Shows the same scenario after 200 years of sea level rise with the lake at a stage of 4.1 m above sea level. As the sea level rises and the lake becomes inundated, fresh groundwater is lost to the lake through evaporation resulting in a decrease in the volume of the freshwater lens.

interpretation. Eventually, the salinity in the lake began to increase again due to the net loss of freshwater from evaporation.

It is also of note that for the high sea level rise simulations, the rate of change in lake salinity is low in the middle of the simulation and relatively high in the beginning and end (Figure 4). This result is related to the geometry of the lake and the hydraulic connection between the lake and the aquifer. At approximately 60 years, the lake expanded, inundating the next layer of grid cells above the original extent of the lake. This mechanism converted the next row of connection grid cells from aquifer cells to lake cells within the Lake Package. The new hydraulic connections between the lake and aguifer allowed fresh groundwater to flow into the lake and temporarily dilute the lake salinity. Later toward the end of the simulation at approximately 150 years, not only did the lake salinity increasing due to evaporation, but as the freshwater lens was depleted, the solute concentration of inflowing groundwater also increased leading to a greater increase in lake salinity.

Overall, these simulations demonstrated the ability of the Lake Transport Package to calculate the transient lake solute concentration due to groundwater inundation from sea level rise under a variety of sea level rise and lake evaporation rates, showing the effect of groundwater induction on freshwater lens depletion. The lake salinity and freshwater lens depletion varied among the scenarios in an intuitive manner. For a given lake evaporation rate, the final lake salinity was greater for the higher sea level rise rate and for a given sea level rise rate, the final lake salinity increased with increasing lake evaporation. This work also demonstrated the ability of the Lake Transport Package to calculate hypersaline lake solute concentrations, as was observed in the extreme lake evaporation/high sea level rise scenario where the final salinity in the lake was 41.6 g/L.

It is important to note, however, that the Lake Transport Package assumes instantaneous and uniform mixing throughout the lake and does not account for lake dynamics, such as stratification. Additionally, these simulations were run for a homogeneous subsurface and more robust testing that includes heterogeneity in the properties that govern the lake-aquifer interaction, such as lakebed leakance, would be beneficial. Future work could involve using the Lake Transport Package to investigate groundwater inundation under several different hydrogeologic settings and lake types found on carbonate platform islands. Although this work focused on the application of the Lake Transport Package to groundwater inundation on an island, the Lake Transport Package can also simulate other situations where variable density flow and transport between a lake, or similar surface water feature, and an aquifer is a significant process. This could include simulating mine waste pits, waste lagoons, or coastal wetlands.

Conclusion

Utilizing the Lake Transport Package can provide a better insight to the effect of groundwater inundation on freshwater resources for small islands. The results from simulations representing groundwater inundation provide a qualitative assessment on the behavior of the Lake Transport Package and demonstrate the ability of this MODFLOW 6 package to calculate the lake solute concentration for transient simulations. Compared to past methods of representing groundwater inundation, the Lake Transport Package provides a method to represent the process in an improved way that is more physically accurate, computationally efficient, and allows for the calculations of lake solute concentration.

Acknowledgments

The authors would like to thank Kalle Jahn of the U.S. Geological Survey and two anonymous reviewers for their constructive comments on the paper. This material is based upon work that is supported by the National Science Foundation (award number 1743370). Any use of trade, firm, or product names is for descriptive purposes only and does not imply endorsement by the U.S. Government.

Authors' Note

The authors do not have any conflicts of interest or financial disclosures to report.

References

- Bakker, M., V. Post, C.D. Langevin, J.D. Hughes, J.T. White,
 A.T. Leaf, S.R. Paulinski, J.D. Larsen, M.W. Toews, E.D.
 Morway, J.C. Bellino, J.J. Starn, and M.N. Fienen. 2021.
 FloPy. U.S. Geological Survey Software Release.
- Bjerklie, D. M., J.R. Mullaney, J.R. Stone, B.J. Skinner, and M.A. Ramlow. 2012. Simulations of the effects of sea-level rise on groundwater levels, New Haven, Connecticut. U.S. Geological Survey Open-File Report 2012-1025.
- Cheng, X., and M.P. Anderson. 1993. Numerical simulation of ground-water interaction with lakes allowing for fluctuating lake levels. *Groundwater* 31, no. 6: 929–933.
- Council, G.W. 1997. Simulating lake-groundwater interaction with MODFLOW. In *Proceedings of the 1997 Georgia Water Resources Conference*, 457–462. Athens, Georgia: The University of Georgia.
- Diersch, H.J.G., and O. Kolditz. 2002. Variable-density flow and transport in porous media: Approaches and challenges. *Advances in Water Resources* 25, no. 8–12: 899–944.
- Ghyben, W.B. 1889. Nota in verband met de voorgenomen putboring nabij Amsterdam (Notes on the Probable Results of the Proposed Well Drilling near Amsterdam), 8–22. The Hague: Tijdschrift Het Koninklijk Instituut Voor Ingenieurs.
- Greskowiak, J. 2014. Tide-induced salt-fingering flow during submarine groundwater discharge. *Geophysical Prospecting* 41: 6413–6419.
- Gulley, J.D., A.S. Mayer, J.B. Martin, and V. Bedekar. 2016. Sea level rise and inundation of Island interiors: Assessing impacts of lake formation and evaporation on water resources in arid climates. *Geophysical Research Letters* 43, no. 18: 9712–9719.

- Guo, W., and C.D. Langevin. 2002. User's guide to SEAWAT: A computer program for simulation of three-dimensional variable-density ground-water flow. U.S. Geological Survey Techniques of Water Resources Investigations 06-A7, 77 p.
- Habel, S., C.H. Fletcher, K. Rotzoll, and A.I. El-Kadi. 2017. Development of a model to simulate groundwater inundation induced by sea-level rise and high tides in Honolulu, Hawaii. *Water Research* 114: 122–134.
- Habtemichael, Y.T., R.T. Kiflemariam, and H.R. Fuentes. 2014. Evaluation of instability of a low-salinity density-dependent flow in a porous medium. In COMSOL Conference, Boston. Burlington, MA: COMSOL, Inc.
- Herzberg, A. 1901. Die Wasserversorgung einiger Nordseebäder (The water supply of some North Sea spas). *Journal Gasbeleucht Wasserversorg* 44, no. 815–819: 842–844.
- Hughes, J. D., C.D. Langevin, and Banta, E. 2017. Documentation for the MODFLOW 6 framework. U.S. Geological Survey Techniques and Methods 6-A57.
- Hunt, R.J., H.M. Haitjema, J.T. Krohelski, and D.T. Feinstein. 2003. Simulating ground water-lake interactions: Approaches and insights. *Groundwater* 41, no. 2: 227–237.
- Konikow, L., D.J. Goode, and G.Z. Hornberger. 1996. A three-dimensional method-of-characteristics solute-transport model (MOC3D): U.S. Geological Survey Water-Resources Investigations Report 96-4267.
- Langevin, C. D., A.M. Provost, S. Panday, and J.D. Hughes. 2022. Documentation for the MODFLOW 6 groundwater transport model. U.S. Geological Survey Techniques and Methods 6-A61, 56 p.
- Langevin, C.D., J.D. Hughes, E.R. Banta, A.M. Provost,
 R.G. Niswonger, and S. Panday. 2021. MODFLOW
 6 Modular Hydrologic Model. U.S. Geological Survey
 Software Release.

- Langevin, C.D., S. Panday, and A.M. Provost. 2020. Hydraulichead formulation for density-dependent flow and transport. *Groundwater* 58, no. 3: 349–362.
- Langevin, C. D., J.D. Hughes, E.R. Banta, R.G. Niswonger, S. Panday, and A.M. Provost. 2017. Documentation for the MODFLOW 6 groundwater flow model, U.S. Geological Survey Techniques and Methods 6-A55, 197 p.
- Langevin, C.D., D.T. Thorne Jr., A.M. Dausman, M.C. Sukop, and W. Guo. 2008. SEAWAT version 4: A computer program for simulation of multi-species solute and heat transport. U.S. Geological Survey Techniques and Methods 6-A22, 39 p.
- Masterson, J.P., M.N. Fienen, E.R. Thieler, D.B. Gesch, B.T. Gutierrez, and N.G. Plant. 2014. Effects of sea-level rise on barrier Island groundwater system dynamics— Ecohydrological implications. *Ecohydrology* 7, no. 3: 1064–1071.
- Merritt, M. L., and L.F. Konikow. 2000. Documentation of a computer program to simulate lake-aquifer interation using the MODFLOW ground-water flow model and the MOC3D solute-transport model. U.S. Geological Survey Water-Resources Investigations Report 00-4167.
- Mulligan, A.E., C. Langevin, and V.E.A. Post. 2011. Tidal boundary conditions in SEAWAT. *Groundwater* 49, no. 6: 866–879.
- Rotzoll, K., and C.H. Fletcher. 2013. Assessment of groundwater inundation as a consequence of sea-level rise. *Nature Climate Change* 3, no. 5: 477–481.
- Schincariol, R.A., F.W. Schwartz, and C.A. Mendoza. 1994. On the generation of instabilities in variable density flow. *Water Resources Research* 30, no. 4: 913–927.